Article:
Chen, M, Goh, SM, Yang, K et al. (8 more authors) (2021) Robust and Flexible Optically Active 2D Membranes Based on Encapsulation of Liquid Crystals in Graphene Oxide Pockets. Advanced Materials Interfaces, 8 (22). 2101432. ISSN 2196-7350

https://doi.org/10.1002/admi.202101432

Robust and flexible two-dimensional optically active membranes.

Encapsulation of liquid crystals in graphene oxide pockets.

*Musen Chen, Shan Min Goh, Kou Yang, Anna A. Nikitina, Siyu Chen, Xuanye Leng, Nazmul Karim, Lindsay Hanson, Helen F. Gleeson, Kostya S. Novoselov and Daria V. Andreeva**

M. Chen, S. M. Goh, K. Yang, S. Chen, X. Leng, Prof. K. S. Novoselov, Prof. D. V. Andreeva
Institute for Functional Intelligent Materials, National University of Singapore, 117544, Singapore
Department of Materials Science and Engineering
National University of Singapore
117575, Singapore
E-mail: daria@nus.edu.sg

A. A. Nikitina
ITMO University
9 Lomonosova street, 191002 St. Petersburg, Russia

Prof. N. Karim
Centre for Fine Print Research
University of West of England
Frenchay Campus, Bristol BS16 1QY, UK

Ms. L. Hanson
Optical Ink
London SE17 1NL, UK

Prof. H. F. Gleeson
School of Physics and Astronomy
University of Leeds
Leeds LS2 9JT, UK

Prof. K. S. Novoselov
Chongqing 2D Materials Institute
Liangjiang New Area, Chongqing 400714, China

Keywords

graphene oxide, reduced graphene oxide, membranes, 5CB, liquid crystals, soft materials, stimuli responsive materials

Abstract

Design and engineering of novel low dimensional metamaterials allow for new applications in membrane technology, aerospace and automotive industries, architecture, robotics, medicine, and textiles. Such materials can be strong, flexible, transparent and can be assigned with different functionalities. Here, we explore the possibility of two-dimensional (2D) graphene oxide (GO) surface to guide self-assembly of 4-cyano-4'-pentylbiphenyl (5CB) molecules via multiple hydrogen bonding and their clustering in optically active phases. The encapsulation of 5CB in a 2D geometry and birefringent properties of 5CB are tuned by the regulation of interaction energy between GO surface and 5CB. Chemical reduction of GO-5CB composites results in electrically conductive rGO-5CB membranes which change optical properties in response to Joule heating. Our sustainable approach to the design of robust and flexible optically active materials will allow the formation of other metamaterials with different functionalities for advanced applications.

1. Introduction

Environmental trends drive the design of new materials that can switch appearance as well as other properties on demand for aerospace and automotive industries, architecture, robotics, medicine, and textiles. It is important to develop new approaches to the formation of robust, flexible, small-footprint and scalable optically active materials that alter the existing environmentally harmful technologies and reduce the use of organic dyes and inorganic pigments.

Large area, macroscopically uniform birefringent films can be prepared by encapsulation of liquid crystals (LCs) into fibers[1a-c] or by their self-assembly into layered polymeric materials.[1d] It was shown that thin films of polymeric LCs or LCs encapsulated into polymer fibers demonstrate excellent performance for applications in gas sensing, wearable devices, smart clothing, etc.[1c, 2] Here, we report on a new approach to self-assembly of two-dimensional (2D) flexible and robust photonic metamaterials consisting of a commercially

available 4-cyano-4'-pentylbiphenyl (5CB) and 2D layers of flexible graphene oxide (GO) and reduced graphene oxide (rGO).

Graphene oxide nanosheets have a unique amphiphilic surface rich in oxygen-containing functional groups, which allows multiple intermolecular bindings such as Van der Waals, hydrophilic/hydrophobic interactions, ionic and hydrogen bonding.[3] Thus, GO possesses good capability to disperse in polar solvents and to form composites.[4] Dispersing GO in 5CB has been utilized to tune the dielectric, electrooptic and optical properties of 5CB.[5] In addition, light-responsive actuators based on polymer-dispersed 5CB/GO composites were reported.[6] In such composites GO-polymer served as soft and flexible scaffold to entrap bulk 5CB phase, and the phase transition of the entrapped 5CB drove the actuation. However, systematic study of the phase transition behaviours of such two-dimensionally confined LCs was yet to be reported. Here, we propose a new approach which allows one to entrap highly organized few layers of 5CB molecules. We use a layer-by-layer vacuum assisted self-assembly approach to precisely control the distribution and orientation of 5CB in highly laminated GO nanolayers. The reveal of phase transition behaviour of GO confined 5CB provides a new perspective for the design of LCs based soft actuators, optically active materials and their inspired new applications.

The vacuum-assisted self-assembly of GO is a simple way to form layered structures. The process involves temporally controlled removal of solvent to achieve the self-organization of 2D flakes driven by Van der Waals attraction and the formation of a perfectly aligned lamellar structure.[7] This process is developed very well for graphene oxide nanosheets alone or in combination with macromolecules.[4b, 8] But the simultaneous assembly of GO flakes with low molecular weight polar molecules such as 5CB remains a challenge due to complex surface induced interactions.

In this work, we develop a physical organic approach to regulate the interactions between GO surface and 5CB molecules through adjustment of solvent, pH and concentration of 5CB. We optimize the preparation conditions to obtain easy-to-handle, robust and flexible membranes that demonstrate the capability to switch optical properties. The fidelity of this approach is demonstrated for 5CB, but it can be adjusted to other small molecules. Upon a direct chemical reduction, we obtain electrically conductive rGO-5CB membranes with a fast response to Joule heating due to their low specific heat. Our membranes have shown potential applications such

as wearable temperature indicators/sensors where consumption of additional energy is not needed. Besides, the conductivity of rGO-5CB membrane will allow for design and fabrication of new smart devices and sensors based on transformation of signals such as electrical current and light.

2. Results and Discussion

The free-standing, optically active 2D composite membranes were prepared through vacuum-assisted self-assembly of GO nanosheets (the mean plane dimension is 6.4 μm) and optically active 4-cyano-4'-pentylbiphenyl (5CB) (a rod-like thermotropic LC with molecular size ~2 nm, see Figure S1). The self-assembly procedure is illustrated in **Figure 1**a. The 5CB/ isopropanol (IPA) solution and GO/H_2O suspension were used. Different ratios of water/IPA were tested to prepare layered membranes of different composition via a vacuum filtration process. As we see in Figure 1b,c, the prepared GO-5CB composite membranes are robust and flexible and have layered morphology.

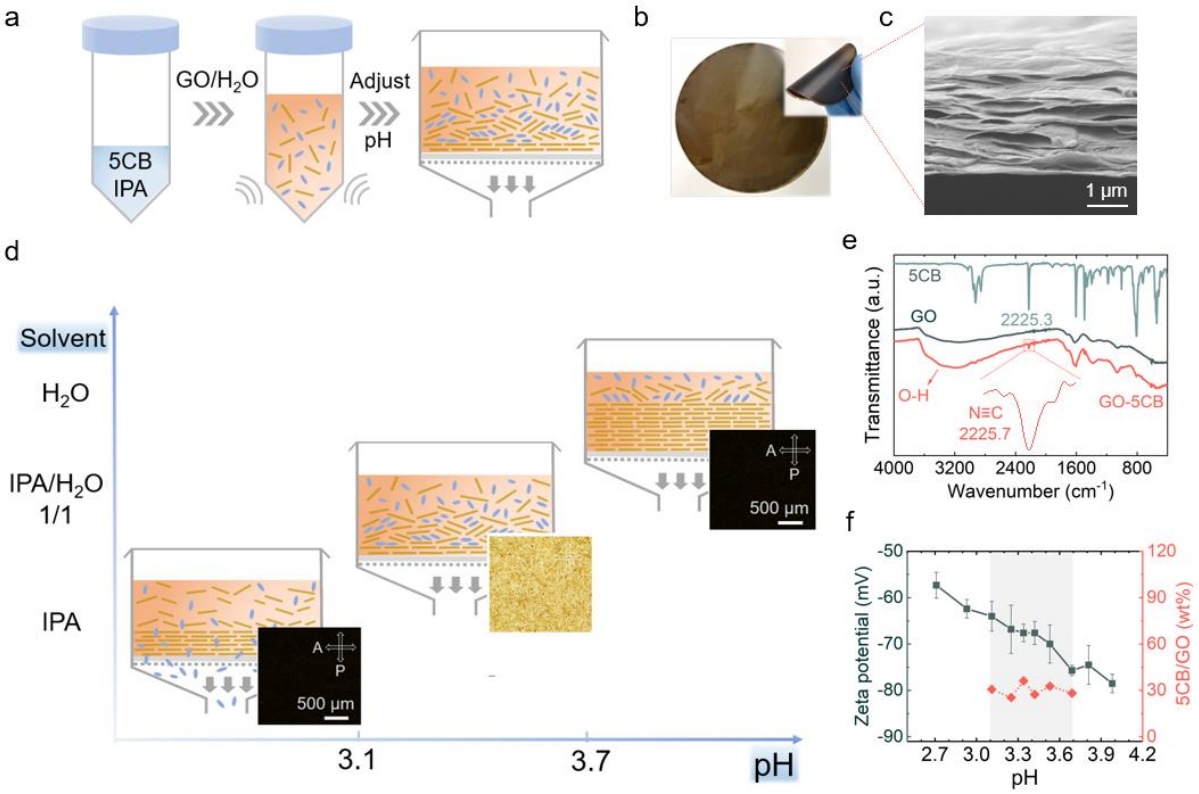

Figure 1. Preparation and characterization of GO-5CB membranes. (a) Sketch of typical preparation procedure of free-standing GO-5CB membranes. (b) Photographs of a GO-5CB membrane with 5CB/GO ratio of 33 wt% prepared at pH 3.5. (c) Scanning electron microscope (SEM) image of cross-sectioned GO-5CB membrane. (d) The diagram illustrates the influence of solvent and pH on the formation of GO-5CB composite membranes. The optical images of the membranes are taken with crossed polariser and analyser. The surfaces of membranes were washed by IPA before imaging. Dark images indicate the absence of birefringent properties, because no 5CB was trapped in GO. All the optical polarizing images have the same scale bar. (e) Attenuated total reflection-Fourier transform infrared spectroscopy (ATR-FTIR) spectra of GO, 5CB and GO-5CB membrane. (f) ζ-potential measurements of GO flakes and 5CB/GO ratios as a function of pH, the shaded area indicates the pH range for the preparation of stable membranes with controllable 5CB loading.

Our task was to find the conditions where interaction potential drives the attachment of 5CB molecules to GO flakes in suspension rather than their dissolution. Such conditions are important to the entrapment of a few layers of LCs and the formation of a macroscopically uniform and stable composite membrane. Figure 1d summarizes the effect of solvent and pH on the encapsulation of 5CB in GO. The upper panel corresponds to the membranes prepared

in water, the lower one – in IPA and the middle one – in water/IPA mixture. The membranes are assembled in the pH range between 2.7 and 4.0.

H_2O is a poor solvent for 5CB. An attempt to disperse 5CB and GO in water leads to bulk phase separation and 5CB accumulating on the surface of water (Figure S2). As shown in Figure 1d (upper panel) due to such phase separation - 5CB molecules form a top layer on the surface of GO membrane in the whole pH range. The good solvent for 5CB is IPA. However, high interaction energy of 5CB with IPA prevents its attachment to the surface of GO. In such case, vacuum-assisted filtration leads to a complete removal of 5CB and IPA (Figure 1d, lower panel) as they go through the filter. In both cases, filtration leads to the formation of pure GO papers rather than composite membranes.

To enhance the interactions between 5CB and GO surface, driving the chemical interaction potential between both components is needed. 5CB is a polar molecule, for the formation of hydrogen bonding, the −CN groups in 5CB can serve as hydrogen acceptors. The −COOH and −OH groups in GO act as hydrogen donors.[3b] The functional groups are highlighted in the attenuated total reflection-Fourier transform infrared spectroscopy (ATR-FTIR) spectra (Figure 1e). Thus, pH can be used to regulate their interactions. The ζ-potential measurements (Figure 1f) show that at pH values between 3.7 to 4.0, the surface of GO is characterized by a larger negative ζ-potential due to a large surface charge density. Such pH values are very close to the pKa of GO (4.2). Therefore, in this pH range GO is partly charged and hydrated. The presence of charged unprotonated functional groups in GO inhibits hydrogen bonding and anchoring of 5CB to the GO surface. At lower pH the surface of GO is characterized by a lower negative ζ-potential. Thus, at lower pH a larger fraction of the GO functional groups is protonated and capable to form hydrogen bonds.

Indeed, as we see in Figure 1d the optically active membranes can be assembled using 1:1 water/IPA solvent in the pH range between 3.1 and 3.7. In such water/IPA mixture the solubility of 5CB molecules is reduced, which makes it easier to attach them to the surface of GO. The ATR-FTIR spectrum of GO-5CB composite (Figure 1e) shows a blue shift for the signal assigned to −CN group, which is an evidence of hydrogen bonding.[9] Using pH in the range between 3.1 and 3.7 allows preparation of membranes with macroscopically uniform mixing of GO and 5CB (Figure 1e and Figure S3). We also studied the influence of the changes of pH on the nematic to isotropic (N-I) phase transition properties (measured by differential

scanning calorimetry, DSC) of 5CB in GO scaffolding. Only small variations of the N-I transition for membranes prepared with constant loading of 5CB but different acidity conditions are observed (Figure S4).

At pH > 3.7, GO-5CB composites are not formed due to a lack of hydrogen bonding. Similarly, at pH < 3.1, membrane formation is prohibited because the multiple Van der Waals interactions between low-charged GO nanosheets lead to the strong GO-GO interactions which repeals 5CB. At such pH we observe a macroscopical phase separation in both the already-formed GO-5CB composite membranes and in the suspensions (Figure S5).

The successfully formed macroscopically uniform GO-5CB membranes exhibit polarizing optical properties. Owing to the optical birefringence of 5CB under nematic state, the N-I phase transition can be observed by optical polarizing microscopy (**Figure 2**). At temperatures below the N-I transition temperature ($T_{N\text{-}I}$) our membranes appear optically bright. When the GO-5CB membrane is heated above the $T_{N\text{-}I}$, the birefringence disappears as 5CB turns into isotropic state. Upon cooling down below the $T_{N\text{-}I}$, the membrane regains the birefringence. The reversibility and isotropic clearing of the N-I transition demonstrate that 5CB phase transition behaviour is not impeded in the membranes. In addition, our mechanical tests indicate that the mechanical stability of membranes is still maintained satisfactory upon encapsulation of 5CB (Figure S6). These properties make our GO-5CB membranes promising for optically active soft materials applications.

Due to self-assembly nature of our composites (5CB molecules are first assembled as a few layers on the surface of GO, due to hydrogen bonding, and 5CB decorated GO flakes are packed together to form laminated membrane structure) our preparation strategy of controlling the hydrogen bonding of 5CB to functional groups of GO as well as of adjustment of solubility of 5CB in the medium allows an accurate adjustment of the membrane composition. We use thermogravimetric analysis (TGA) data to calculate the 5CB fractions in GO membranes depending on 5CB loading (Figure S7). As evident in Figure S7, the fraction of 5CB in the membrane is linearly dependent on the 5CB concentration added to the dispersion during preparation.

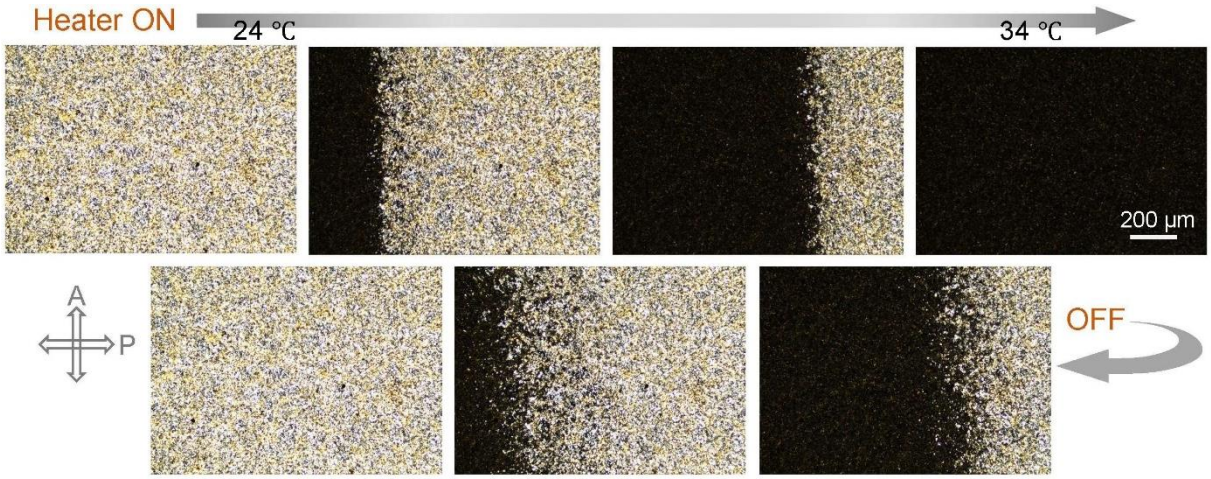

Figure 2. Optical polarizing images show the reversible 5CB phase transition in GO-5CB membrane in response to external heating (from 24 °C to 34 °C with 5 °C min^{-1} heating rate).

The scanning electron microscope (SEM) cross section image of GO-5CB membrane (Figure 1c) shows that the membrane consists of the pockets with sub-micron thickness randomly distributed in the membrane. 5CB molecules are entrapped in such nano-sized pockets rather than homogeneously distributed along 2D layers (see X-ray diffractometer (XRD) data in Figure S8). Microscopic dewetting was used to explain thickness fluctuations in LC films.[10] Due to strong polarity of LC molecules a strongly polar substrate is required for the preparation of homogeneous films and to achieve complete wetting. Thus, the pocket-like distribution of LCs on chemically inhomogeneous GO surface can be explained by the strong cohesion resulting from the long-range dipolar forces.[10] **Figure 3**a illustrates two GO pockets with large and small fraction of 5CB. The encapsulation of 5CB into GO pockets provides both the formation of large area, macroscopically uniform birefringent membranes due to the uniform distribution of nano-pockets and excellent stability and flexibility of Van der Waals GO structure.

To reveal the effect of GO pockets on the orientation and distribution of 5CB, we measure the thermal properties of the samples with different 5CB loading. The DSC curves of bulk 5CB show a sharp peak at 33.4 °C (Figure 3b). In contrast, the curves for 5CB encapsulated in GO show that, the transition peaks are broadened and shifted downward (until 31.1 °C) (Figure 3b,c) and are more symmetric. Similar tendency was observed for 5CB confined in electrospun fibers,[11] and in nanopores,[12] with decrease of the fiber or pore size. We would like to point

out that the broadening of the transition peaks is significantly smaller than the peak shift, as compared to bulk 5CB.

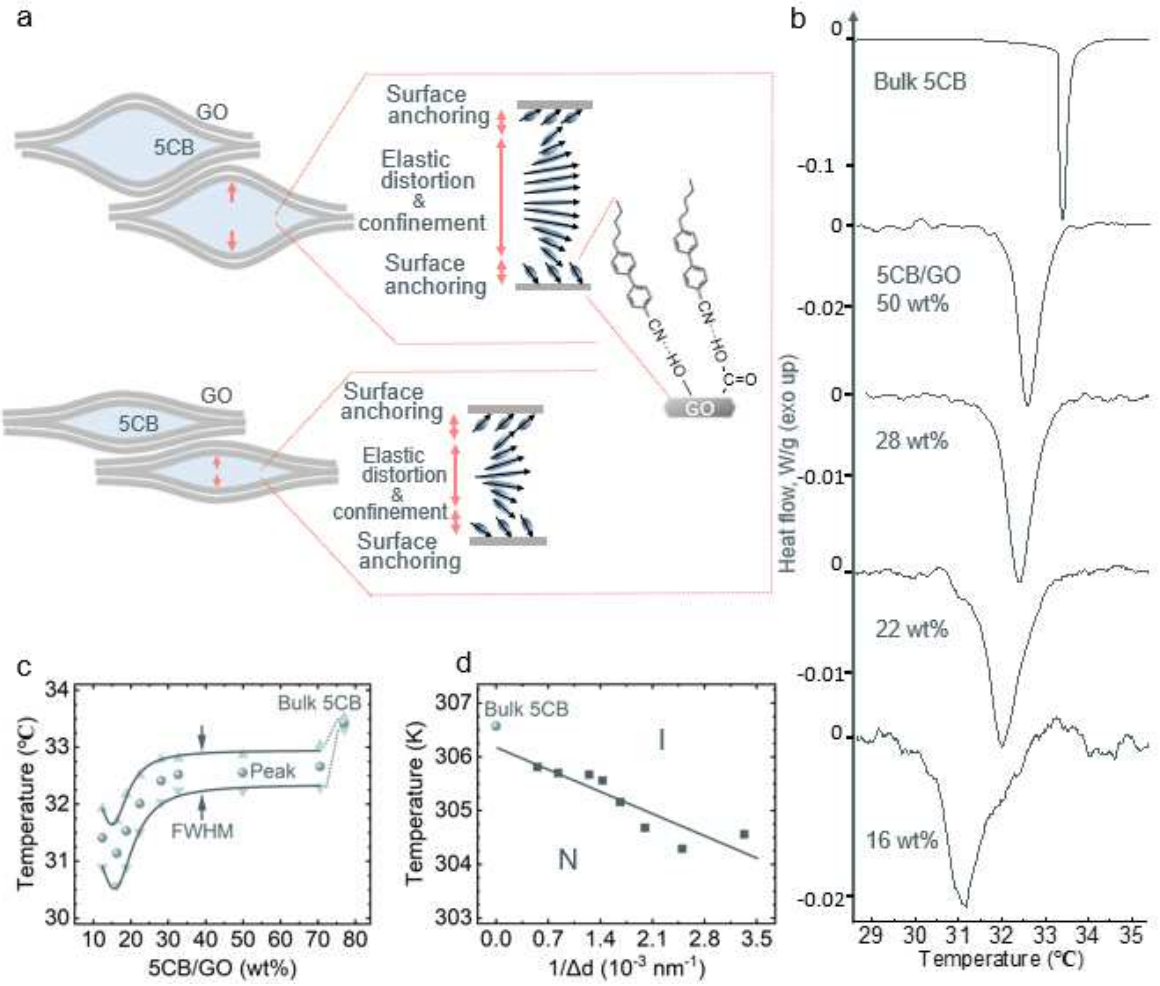

Figure 3. Phase transition properties of GO confined 5CB. All the membranes were prepared at pH 3.5. (a) Schematic illustration of 5CB confined in GO pockets with different size. (b) The baseline subtracted DSC curves of bulk 5CB and membranes with different 5CB loading. (c) Peak positions and full width at half maximum (FWHM) extracted from DSC curves as a function of 5CB/GO weight ratio; the FWHM was obtained by Gauss fitting; the solid lines are a guide to the eye. (d) Dependence of the transition temperatures of GO confined 5CB plotted as a function of the inverse membrane thickness increment ($1/\Delta d$) compared to bare GO membrane (2.0 μm).

To understand this behaviour as well as the orientational structure of 5CB in GO, we note that the successfully formed GO-5CB composites exhibit optical polarization properties below $T_{N\text{-}I}$: it is optically bright when observed under crossed-polarised condition (Figure 2). This

suggests that below the T_{N-I} a significant portion of 5CB molecules are tilted out the direction of the vertical light beam and oriented along the planar direction of GO layers. Reduction of the transition temperature for 5CB confined in GO is associated with the formation of the surface anchoring layer and its influence, which induces the elastically distorted 5CB orientational structure in the interior of the pocket.[13] In the anchoring layer, hydrogen bonding between 5CB and GO orients 5CB to a homeotropic alignment (perpendicular to the GO layer, as illustrated in Figure 3a). This forms a transition structure in the interior of the pocket where 5CB molecules gradually rotates from homeotropic at the anchoring layer to planar in the middle of the pocket.

The fact that the shift of the N-I transition peak of GO confined 5CB is larger than its broadening (compared to bulk 5CB, see Figure 3b,c) suggests that, the thickness of the GO confined 5CB droplets is smaller than the characteristic distance at which elastic distortion disappears, so we observe a new type of phase transition for a distorted structure. The larger the level of distortion in such structure (happens in thinner pockets at low 5CB fraction) – the larger is the shift of the transition temperature. In thinner pockets the relative contribution of the influence of surface-anchoring layer is larger – which also contributes to the reduction of the transition temperature. We also expect the formation of a multidomain nematic structure caused by such confinement, elastic distortion and surface interaction, which may be related to multiple peaks obtained by peak fitting of the DSC curves (Figure S9).

Following previous work,[12] we plot T_{N-I} as a function of inverse membrane thickness increment ($1/\Delta d$) compared to bare GO membrane (Figure 3d). We see that the T_{N-I} reduces linearly with the inverse membrane thickness increment, which can be parametrized as T_{N-I} [K] = 306.2 [K] - 587/Δd[nm]. Similar linearity was observed previously for 5CB confined in nano-sized pores by both DSC and dielectric spectroscopy (DS).[12]

It is expected that the response of the membrane can also be achieved through self-generation of heat by Joule effect driven by electrical current (**Figure 4**). To obtain electrically conductive and optically transparent membranes, we reduced GO-5CB (1-μm-thick) to rGO-5CB in ascorbic acid (Figure S10). Upon reduction, we obtained rGO-5CB membrane with sheet resistance of approx. 10 kΩ sq^{-1} and 5CB loading of 0.34 mg cm^{-2}. The successful reduction was further justified by ATR-FTIR, Raman spectroscopy and TGA (see Figure S10, S11). The

transition temperature $T_{N\text{-}I}$ after the reduction stays approximately the same, as confirmed by DSC and cross-polarised microscopy imaging under varying temperature.

An electrical current responsive device is shown in Figure 4a. By applying a voltage, the current flows through the conductive rGO matrix, generating Joule heating to trigger the N-I transition of 5CB (Figure 4c). The switching time depends on a number of factors – the heat capacitance of the device and the substrate, the thermal conductivity of the substrate, the temperature of surrounding atmosphere. The most fundamental limitation is given by the specific heat of the N-I phase transition. Based on DSC and TGA measurements (Figure S11), the heat of N-I transition for the rGO-5CB membrane is calculated to be 1.9 J g^{-1}. To demonstrate the fast switch capability of our device, we calculate the theoretical switch time (regardless of heat loss and temperature dependent resistance of rGO[14]) as a function of area of square sample and applied voltage (Figure 4b). It is seen that the transition of a 2 × 2 cm sample can be switched within 1 second when a voltage of only 5 V is applied.

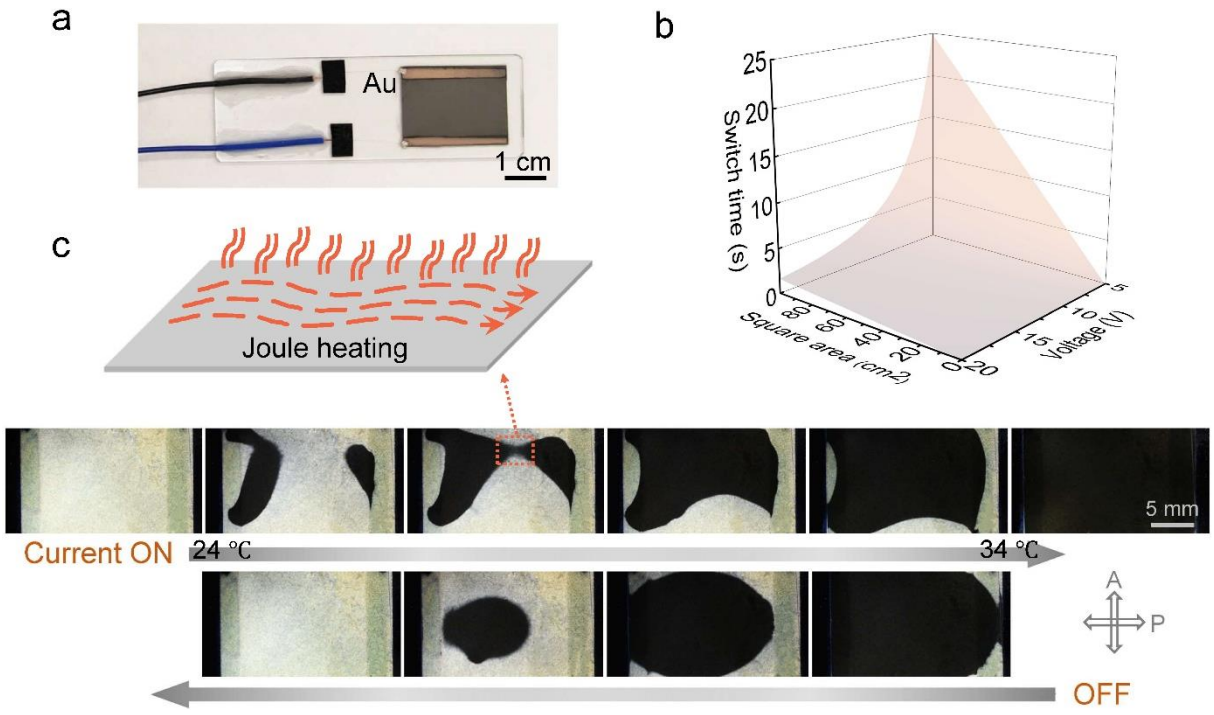

Figure 4. Electrical current responsive device based on rGO-5CB membrane. (a) Photograph of a device with membrane resistance of 10 kΩ sq^{-1} and 5CB loading of 0.34 mg cm^{-2}. The substrate is a glass slide and the electrodes are 10 nm deposited gold. (b) Calculated theoretical switch time of a square sample as a function of sample area and voltage applied. (c) Optical polarizing images showing the reversible 5CB phase transition in the membrane, the response

to electrical current is achieved by self-heating via Joule effect. Applied current for the top row of images is 7 mA. The duration of the switching is 1 min.

3. Conclusion

We developed a new self-assembly strategy for the encapsulation of 5CB in GO nanolayers. The regulation of interfacial interactions is important for the preparation of robust and flexible optically active 2D membranes. We adjusted solvent and pH to formulate the optimal self-assembly conditions. Regulation of 2D confinement of LCs is the major factor for tuning phase transitions of 5CB. The mechanism involves the contribution of multiple hydrogen bonding of 5CB molecules to GO surface, surface induced microscopic dewetting and encapsulation of 5CB in GO pockets, elastic distortion of 5CB in 2D confinement. We elucidated surface effects in 2D geometries for self-orientation of liquid crystals and tuning optical properties on demand. Furthermore, we fabricated the device that can be digitally switched on/off. Our approach is versatile and adjustable for finishing of a variety of surfaces from metals, plastics to textiles, wood and concrete.

4. Experimental Section

Materials: Aqueous graphene oxide dispersion (4 mg mL^{-1}, monolayer content > 95%, GO oxygen content 41-50%, Graphenea Inc., USA), 4-cyano-4'-pentylbiphenyl (5CB, nematic, 98%, Sigma-Aldrich), Isopropanol (IPA, 99.8%, Fisher Scientific), Anodisc^{TM} 47 aluminium oxide filter (pore size 0.02 μm, diameter 47 mm, Whatman), Hydrochloric acid (37%, ACS reagent, Sigma-Aldrich), Ascorbic acid (ACS reagent, Sigma-Aldrich), Silver conductive glue (RS Components, UK). All the chemicals were used without additional purification.

Preparation of GO-5CB composite membranes: In a typical preparation, 5CB was dissolved into IPA (10.0 mL) before mixed with GO/H_2O (10.0 mL, 0.3 mg mL^{-1}, directly diluted from 4 mg mL^{-1}). The mixture had a natural pH of 4 (measured by pH meter, SevenExcellence, Mettler-Toledo (S) Pte. Ltd.). After pH adjustment by hydrochloric acid, it was sonicated for 5 min (40 kHz ultrasonic bath, 0.04 W mL^{-1}, the sonochemical effect here on GO composition was negligible) and then was poured into the vacuum-assisted filtration assembly to form membrane. The filtration process took around 15-20 h, thus the funnel was sealed to avoid the disturbance of solvent evaporation. Unless specified, all the membranes have GO of 0.265 mg cm^{-2}.

Reduction of GO-5CB composite membranes: To gain a sufficient optical transparency of a reduced GO-5CB membrane, the use of GO content below 0.14 mg cm^{-2} is recommended. In this work, we first prepared a thin GO-5CB membrane by the above typical approach using 15 μL 5CB, 3.5 mL IPA, 3.5 mL 0.34 mg mL^{-1} GO/H_2O, and pH around 3.5. Then, it was directly reduced by soaking in ascorbic acid aqueous solution (15 mL, 30 mg mL^{-1}) in 70 °C for 24 h. After reduction, the membrane surface was carefully rinsed by DI water. For preparation of thin GO-5CB membranes, increased amount of 5CB and decreased total volume of solvent are needed for successful encapsulation of 5CB with less GO.

Fabrication of rGO-5CB membrane based device: The rGO-5CB membrane was stuck onto a glass slide by fishing with DI water and dried in dry cabinet. The surfaces along its two edges were gold sputtered (10 nm) and connected to conductive wires by silver conductive glue. A source meter (6430 Sub-Femtoamp Remote SourceMeter®, Keithley) was used as power source.

Instrumental characterizations: The optical microscope (Nikon Eclipse LV100ND) with digital camera and imaging software (NIS-Elements) was utilized to record the optical polarizing images of the samples, in which glass slide was used as substrate. The membrane chemical components were identified by attenuated total reflection-Fourier transform infrared spectroscopy (ATR-FTIR, IRTracer-100, Shimadzu) in range of 400-4000 cm^{-1} with 4 cm^{-1} resolution. The zeta potential of GO flakes was measured by Zetasizer (ZSU5700, Malvern Panalytical). The flake size of GO and membrane structure were investigated by scanning electron microscope (SEM, Zeiss Sigma 300); the membrane samples were gold sputtered (~ 5 nm) before observation, the fracture edge for cross-section imaging was obtained by applying in-plane strain to the membrane. The membrane average thickness was measured by Alpha-Step IQ Surface Profiler (KLA Tencor). The GO d-spacing was calculated by Bragg's law [$\lambda=2d\sin(\theta)$] based on patterns (θ was extracted by Gauss fitting) obtained from X-ray diffractometer (XRD, Bruker D8 Advance), with Cu Kα radiation wavelength (λ) of 1.5418 Å, 0.02° increment and 1 s per step. Raman spectroscopy (WITEC ALPHA300R, 532 nm laser). The mechanical analysis was performed using home-made sample holders and a testing system (Instron 3345) with 10 N load cell, the membranes were cut into rectangular strips with width of 9.0 mm and tested at room temperature with displacement rate of 0.5 mm min^{-1}. The phase transitions of 5CB were studied by differential scanning calorimetry (DSC 25, TA Instruments) with 1 °C min^{-1} heating rate and 50 mL min^{-1} N_2 flow rate. The thermal stability and component

content were analysed by thermogravimetric analysis (TGA, Q500, TA Instruments) with 20 °C min^{-1} ramping and 60 mL min^{-1} N_2 purging rate.

Supporting Information

Supporting Information is available from the Wiley Online Library or from the author.

Acknowledgements

This work was supported by the Ministry of Education (Singapore) through the Research Centre of Excellence program (grant EDUN C-33-18-279-V12, I-FIM). AN thanks to the RSF (Russian Federation) grant no. 19-19-00508. KSN acknowledges support from EU Graphene Flagship Program (contract CNECTICT-604391), European Research Council Synergy Grant Hetero2D, the Royal Society, EPSRC grant EP/N010345/1.

Conflict of Interest

The authors declare no conflict of interest.

Received: ((will be filled in by the editorial staff))
Revised: ((will be filled in by the editorial staff))
Published online: ((will be filled in by the editorial staff))

References

[1] a) E. Bukusoglu, M. Bedolla Pantoja, P. C. Mushenheim, X. Wang, N. L. Abbott, *Annu. Rev. Chem. Biomol. Eng.* **2016**, *7*, 163; b) H. K. Bisoyi, Q. Li, *Chem. Rev.* **2016**, *116*, 15089; c) M. Urbanski, C. G. Reyes, J. Noh, A. Sharma, Y. Geng, V. S. R. Jampani, J. P. F. Lagerwall, *J. Phys.: Condens. Matter* **2017**, *27*, 133003; d) V. Cherpak, V. F. Korolovych, R. Geryak, T. Turiv, D. Nepal, J. Kelly, T. J. Bunning, O. D. Lavrentovich, W. T. Heller, V. V. Tsukruk, *Nano Lett.* **2018**, *18*, 6770.

[2] D. K. Kim, M. Hwang, J. P. F. Lagerwall, *J. Polym. Sci., Part B: Polym. Phys.* **2013**, *51*, 855.

[3] a) J. Kim, L. J. Cote, F. Kim, W. Yuan, K. R. Shull, J. Huang, *J. Am. Chem. Soc.* **2010**, *132*, 8180; b) D. R. Dreyer, S. Park, C. W. Bielawski, R. S. Ruoff, *Chem. Soc. Rev.* **2010**, *39*, 228.

[4] a) J. I. Paredes, S. Villar-Rodil, A. Martínez-Alonso, J. M. D. Tascón, *Langmuir* **2008**, *24*, 10560; b) S. Chen, K. Yang, X. Leng, M. Chen, K. S. Novoselov, D. V. Andreeva, *Polym. Int.* **2020**, *69*, 1173.

[5] a) S. Al-Zangana, M. Iliut, M. Turner, A. Vijayaraghavan, I. Dierking, *Adv. Opt. Mater.* **2016**, *4*, 1541; b) M. Mrukiewicz, K. Kowiorski, P. Perkowski, R. Mazur, M. Djas, *Beilstein J. Nanotechnol.* **2019**, *10*, 71; c) S. Yadav, P. Malik, Khushboo, D. Jayoti, *Liq. Cryst.* **2020**, *47*, 984; d) S. Al-Zangana, M. Iliut, G. Boran, M. Turner, A. Vijayaraghavan, I. Dierking, *Sci. Rep.* **2016**, *6*, 31885.

[6] a) Z. Cheng, T. Wang, X. Li, Y. Zhang, H. Yu, *ACS Appl. Mater. Interfaces* **2015**, *7*, 27494; b) L. Yu, Z. Cheng, Z. Dong, Y. Zhang, H. Yu, *J. Mater. Chem. C* **2014**, *2*, 8501.

[7] D. A. Dikin, S. Stankovich, E. J. Zimney, R. D. Piner, G. H. B. Dommett, G. Evmenenko, S. T. Nguyen, R. S. Ruoff, *Nature* **2007**, *448*, 457.

[8] D. V. Andreeva, M. Trushin, A. Nikitina, M. C. F. Costa, P. V. Cherepanov, M. Holwill, S. Chen, K. Yang, S. W. Chee, U. Mirsaidov, A. H. Castro Neto, K. S. Novoselov, *Nat. Nanotechnol.* **2021**, *16*, 174.

[9] P. Deb, T. Haldar, S. M. Kashid, S. Banerjee, S. Chakrabarty, S. Bagchi, *J. Phys. Chem. B* **2016**, *120*, 4034.

[10] S. Herminghaus, K. Jacobs, K. Mecke, J. Bischof, A. Fery, M. Ibn-Elhaj, S. Schlagowski, *Science* **1998**, *282*, 916.

[11] K. T. Dicker, D. Ratchford, R. Casalini, M. D. Thum, J. H. Wynne, J. G. Lundin, *Langmuir* **2020**, *36*, 7916.

[12] C. Grigoriadis, H. Duran, M. Steinhart, M. Kappl, H.-J. Butt, G. Floudas, *ACS Nano* **2011**, *5*, 9208.

[13] G. S. Iannacchione, D. Finotello, *Phys. Rev. Lett.* **1992**, *69*, 2094.

[14] S. Lai, M. Chen, Y. N. Khanin, K. S. Novoselov, D. V. Andreeva, *Surf. Rev. Lett.* 2021, *28*, 2140011.